Clay Minerals, (2018) **53**, 393–402

Investigation, using density function theory, of coverage of the kaolinite (001) surface during hydrogen adsorption

JIAN ZHAO[1,2], WEI GAO[1,2], ZHI-GANG TAO[1,2,*], HONG-YUN GUO[3] AND MAN-CHAO HE[1,2]

[1] *State Key Laboratory of Geomechanics and Deep Underground Engineering, University of Mining and Technology, Beijing 100083, China*
[2] *School of Mechanics and Civil Engineering, University of Mining and Technology, Beijing 100083, China*
[3] *Beijing Special Engineering Design and Research Institute, Beijing 100028, China*

(*Received 7 December 2017; revised 26 May 2018; Guest Associate Editor: Ignacio Sainz Diaz*)

ABSTRACT: Kaolinite can be used for many applications, including the underground storage of gases. Density functional theory was employed to investigate the adsorption of hydrogen molecules on the kaolinite (001) surface. The coverage dependence of the adsorption sites and energetics was studied systematically for a wide range of coverage, Θ (from 1/16 to 1 monolayer). The three-fold hollow site is the most stable, followed by the bridge, top-z and top sites. The adsorption energy of H_2 decreased with increasing coverage, thus indicating the lower stability of surface adsorption due to the repulsion of neighbouring H_2 molecules. The coverage has obvious effects on hydrogen adsorption. Other properties of the H_2/kaolinite (001) system, including the lattice relaxation and changes of electronic density of states, were also studied and are discussed in detail.

KEYWORDS: clay minerals, kaolinite, hydrogen, adsorption, first-principles calculations, density functional theory.

Serious environmental problems including global warming and local pollution are associated directly with excessive usage of fossil fuels (Fayaz *et al*., 2012; Xie *et al*., 2014). 'Green' energy to replace fossil fuels has become most challenging energy issue of the last few decades (Roszak *et al*., 2016; Shervani *et al*., 2017). Hydrogen is a promising candidate as an energy source due to its high energy density per unit mass and availability; because hydrogen can be produced from renewable resources *via* photoelectrochemical and biological processes, it has minimal environmental impact (Zhang *et al*., 2014; Ren *et al*., 2017). Storage is an important step in the utilization of hydrogen as a green fuel (Mondelli *et al*., 2015). The potential for safe and affordable storage of hydrogen in materials has attracted considerable attention recently (Hörtz *et al*., 2015; Alver, 2017; Wei *et al*., 2017). Among the various storage methods, adsorption is one of the most popular because it is simple to use (Niaz *et al*., 2015). Therefore, many investigators have studied the storage of H_2 experimentally using chemical and physical adsorption in different materials, including metals (Sun *et al*., 2016; Bachurin & Viadimirov, 2017), alloys (Mahdi & Sahar, 2015), minerals (Arean *et al*., 2009; Henkel *et al*., 2014; Sigot *et al*., 2016) and organometallic compounds (Gu *et al*., 2004). Concerning sorbent materials, natural or modified clay minerals have received much attention as possible low-cost and high-thermal-stability adsorbents in the storage of H_2 removed from contaminated air

*E-mail: taozhigang@263.net
https://doi.org/10.1180/clm.2018.28

(Itadania *et al*., 2007; Charlet *et al*., 2017). Kaolinite is one of the most abundant clay minerals (Brigatti *et al*., 2006; Chen & Lu, 2015) and is very common in soils, especially in tropical and sub-tropical areas. The storage of H_2 on kaolin clays is based on an adsorption mechanism. The use of kaolinite to adsorb gases such as hydrogen, water and carbon dioxide has been reported in the past (Venaruzzo *et al*., 2002; Saada *et al*., 2003). Cations on kaolinite surfaces create a strong electric field that favours gas adsorption. So far, experimental methods of adsorption usually provide enthalpies and sometimes equilibrium constants, but they do not provide information about the geometry of adsorption on the sorbent. A theoretical analysis of the adsorption mechanism of H_2 monomers on natural kaolinite from a microscopic point of view would improve understanding of the adsorptive properties of the kaolinite–H_2 interface and the influence of H_2 adsorbed on clay minerals. Computational chemistry calculations based on density functional theory (DFT) have proven to be a powerful and reliable tool to study H_2–solid interfaces at the microscopic level. Hence, a greater insight into the process of H_2 adsorption on the kaolinite (001) surface through detailed first-principles analysis is necessary.

Existing experimental data (Adams, 1983; Bish, 1993; Benco *et al*., 2001), calculated results (Hess & Saunders, 1992; Hayashi, 1997; Hobbs *et al*., 1997; Plançon & Giese, 1997; Teppen *et al*., 1997; Hu & Michaelides, 2008) and data on the kaolinite layers with the ideal structural formula $Al_2Si_2O_5(OH)_4$ are based on the 1:1 layer structure, consisting of a tetrahedral (SiO_4) sheet in which Si atoms are coordinated by oxygen anions and an octahedral (AlO_6) sheet where Al atoms are coordinated by oxygen atoms and hydroxyl groups (Bailey, 1980). Quantitative estimates indicate that there is a certain degree of van der Waals attraction and hydrogen bonding between the silicate (SiO_4) sheet and the adjoining aluminate (AlO_6) sheets (Sato *et al*., 2005; Hajjaji *et al*., 2016). Kaolinite microparticles exist as hexagonal plates with dominant (001) basal surfaces that are almost perfectly cleaved; this is the plane that is mainly exposed in kaolinite crystals (Giese, 1973; Šolc *et al*., 2011). As reported by Zhang *et al.* (2014), the hydroxyl groups of the Al–O surface are supposed to form hydrogen bonds with molecules such as water and carbon dioxide (Hu & Michaelides, 2008; He *et al*., 2014). Thus, the hydroxyl (001) surface is the surface of primary interest in adsorption studies. Calculations were also performed to determine the adsorption energy of hydrogen molecules on the tetrahedral ($00\bar{1}$) and hydroxylated (001) surfaces of kaolinite. The results showed that a hydrogen molecule adsorbs more weakly on the tetrahedral surface than it does on the octahedral surface. The objectives of this study were to investigate H_2 adsorption sites, adsorption energies, charge transfer, H_2 structure during adsorption and the structure of the intermediate reaction complex.

METHOD OF CALCULATIONS

Periodic DFT calculations were performed using the frozen-core all electron projector augmented wave method in the Vienna *ab initio* simulation package (VASP) (Kress & Furthmüller, 1996). The Kohn–Sham DFT equations were solved using plane-wave pseudopotentials and periodic boundary conditions. The local density approximation of electron exchange potential and correlation energy was used. The electron–ion interaction is described by Blöchl's projector augmented wave method, which takes the exact shape of the valence wave functions into account (Blöchl, 1994; Kresse & Joubert, 1999). The converged kinetic energy cut-off was set to 400 eV, which was sufficient to ensure that the error is <0.01 eV in the calculated values for energies and <0.001 Å for the primitive bulk cell. Monkhorst–Pack meshes (Monkhorst & Pack, 1976) of a 3 × 3 × 1 k-point grid in the Brillouin surface for the *p* (2 × 2) surface cell were used.

The kaolinite (001) surface was modelled using a slab composed of 'H–O–Al–O–Si–O' six atomic sublayers with a vacuum thickness of 20 Å. Based on the data of Hess and Saunders (1992), the calculated lattice parameters of bulk kaolinite were $a = 5.155$ Å, $b = 5.155$ Å, $c = 7.405$ Å, $\alpha = 75.14°$, $\beta = 84.12°$ and $\gamma = 60.18°$, and these were used in the present study. Adsorbates were placed on one side of the slab and a dipole correction was included for all slab calculations. During the calculation, all the H, O and Al atoms in the three sublayers (AlO_6 surface), as well as the H_2, were allowed to relax while the other three atomic sublayers (SiO_4 surface) of the slab were kept fixed at the calculated bulk positions. In the present study, calculations for adsorbed H_2 molecules at surface coverages that ranged from 1/16 to 1 monolayer (ML) were performed for nine adsorption sites. With regards to the inner-surface hydroxyl groups, the nine adsorption sites included three one-fold top sites (T_1–T_3), two two-fold bridge sites (B_1–B_2) and four three-fold cavity sites (H_1–H_4). Figure 1 shows the hydroxylated (001) surface of kaolinite after relaxation, in which two-thirds of the surface hydroxyl

https://doi.org/10.1180/clm.2018.28 Published online by Cambridge University Press

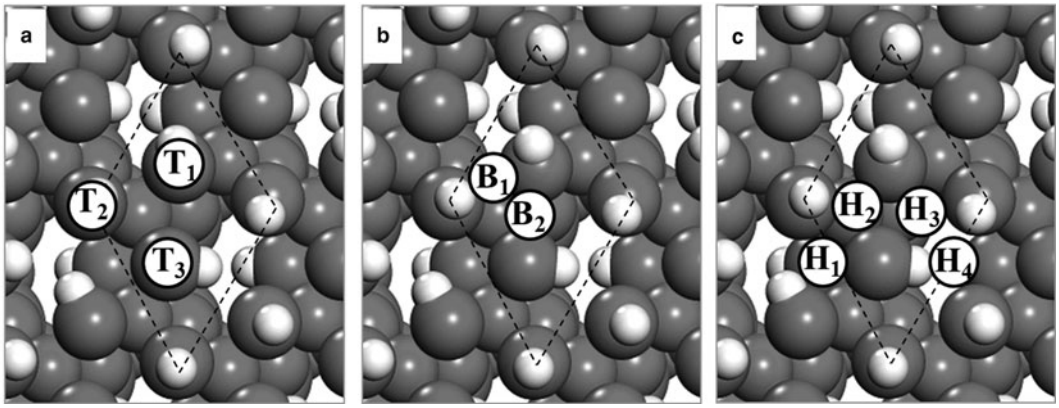

FIG. 1. Top view of kaolinite (001) surface with (a) three top adsorption sites (T_1–T_3), (b) two bridge adsorption sites (B_1–B_2) and (c) four cavity adsorption sites (H_1–H_4).

groups tilt (T_1–T_2) and the other third of hydroxyl groups are almost parallel (T_3) to the surface. The adsorption of H_2 on the cavity sites for 1/16, 1/8, 1/4, 1/2, 3/4 and 1 ML with the p (2 × 2) surface cell and the coverage of 1/8, 1/4, 1/2, 3/4 and 1 ML of H_2 molecules on the top and bridge sites were calculated systematically, respectively. Several sizes of the kaolinite (001) model were used to test the influence of model size on H_2 adsorption energy.

RESULTS AND DISCUSSION

In the present study, the adsorption energy (E_{ads}) is the average adsorption energy of the H_2 molecules on kaolinite substrate, defined as

$$E_{ads}(\Theta) = -\frac{1}{N_{H_2}}[E_{H_2/kaolinite(001)} - E_{kaolinite(001)} - N_{H_2}E_{H_2}] \quad (1)$$

where $E_{H_2/kaolinite(001)}$ and $E_{kaolinite\ (001)}$ are total energies of an N hydrogen adsorption system and the corresponding clean kaolinite surface, respectively. E_{H_2} is the total energy of a free hydrogen molecule, N_{H_2} is the total number of hydrogen molecules adsorbed and Θ is defined as the ratio of the number of H_2 molecules adsorbed to the total number of molecules adsorbed on the corresponding top, bridge or cavity sites in an ideal kaolinite (001) surface. With this definition, a positive value of the adsorption energy indicates that the adsorption is an exothermic (stable) process and a negative value indicates an endothermic (unstable) reaction. Similar to Hu and Michaelides (2008), all of the three kinds of high-symmetry adsorption sites on the (001) surface were considered. Two original molecular configurations of upright and recumbent CH_4 with respect to the surface were examined at all adsorption sites. After optimizing the adsorption models, the three adsorption states of the top (T_1–T_3), bridge (B_1–B_2) and cavity sites (H_1–H_4) with tilted (Figs 2a, c, d) or perpendicular (Fig. 2b) H_2 molecules were stabilized. The H–H bond of adsorbed H_2 molecules on the top (T_3) adsorption sites is perpendicular to the surface (named as top-z for clarity) after relaxation, and the remainder form acute angles with the surface. The perpendicular and tilted orientation represented configurations in which one hydrogen atom of H_2 formed a bond with the surface. All top (T_1–T_2), bridge (B_1–B_2) and cavity (H_1–H_4) adsorption sites for H_2 molecules had similar adsorption energies in the coverage regime of $0 < \Theta \leq 1$ ML, respectively. The calculated adsorption energies (E_{ads}) of H_2 on these four types of surface sites with respect to the free molecule H_2 are summarized and illustrated for different H_2 coverages for $0 < \Theta \leq 1$ ML (Fig. 3; Table 1).

A tilted H_2 on the cavity site at a coverage of 1/16 ML was energetically stable, followed in order of reducing stability by tilted H_2 on the bridge and the top (T_1–T_2) sites at a coverage of 1/8 ML. Here, the adsorption energies of H_2 on the kaolinite (001) surface were 0.17, 0.28 and 0.39 eV for the top (T_1–T_2), bridge and cavity sites, respectively. The adsorption energy of the H_2 molecule on the T_3 (top-z) site was 0.22 eV at $\Theta = 1/4$ ML, which was higher than the top (T_1–T_2) sites but lower than the bridge and cavity sites. At the highest coverage of 1 ML, an inclined H_2 molecule was preferably adsorbed on the cavity site,

https://doi.org/10.1180/clm.2018.28 Published online by Cambridge University Press

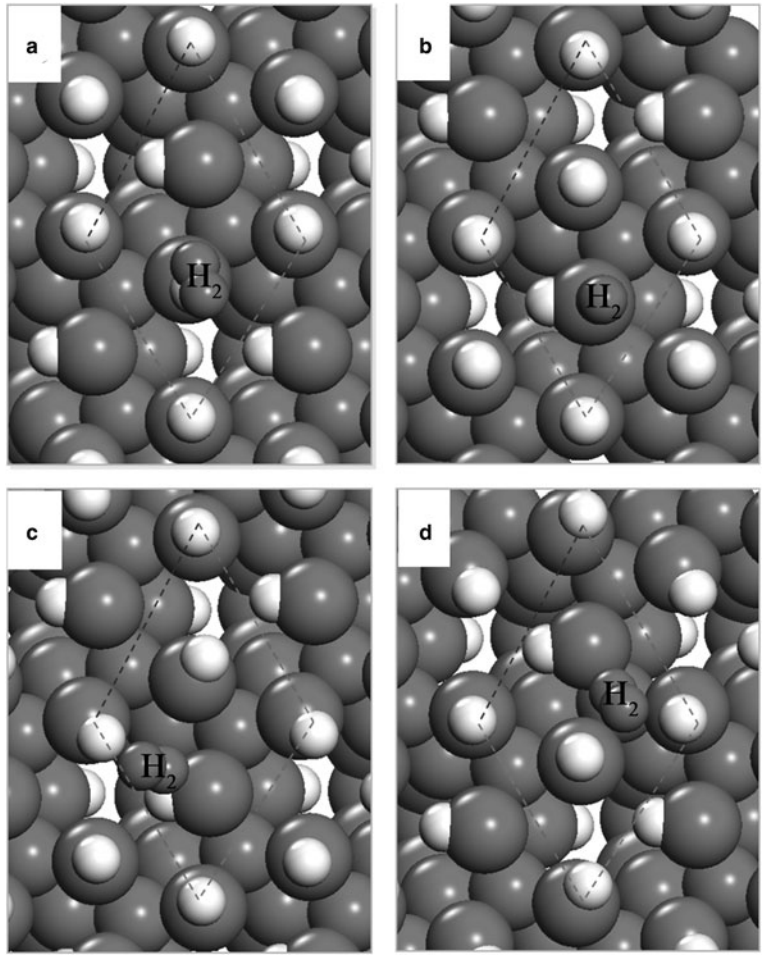

FIG. 2. Top view of H_2 molecule adsorbed on the (a) top, (b) top-z, (c) bridge and (d) cavity sites of kaolinite (001) surface.

and the following stable adsorption sites were the bridge, top-z and top sites. The adsorption energies of H_2 on the kaolinite (001) surface were 0.14, 0.18, 0.20 and 0.26 eV for the top, top-z, bridge and cavity sites, respectively. The calculated adsorption energies of H_2 (Fig. 3) revealed that the cavity site was more stable than the bridge, top-z and top sites in the coverage regime of $0 < \Theta \leq 1$ ML. Meanwhile, the quantities of the top, top-z, bridge and cavity adsorptions displayed a modestly decreasing tendency with the increase in H_2 adsorption, while the overall variation of the magnitude of E_{ads} was rather small in the range of coverage. The decrease in adsorption with coverage indicated lower stability of surface adsorption due to the repulsion of neighbouring H_2 molecules.

Calculated geometries for H_2 molecule adsorption on the top, top-z, bridge and cavity sites of kaolinite (001) at $\Theta = 1/4$, 1/2, 3/4 and 1 ML, including the H–H bond lengths d_{H-H} (Å), the angle of the H–H bond with the surface (∠HHS) in degrees and the height h_{H_2-H} of adsorbate H_2 above the (001) surface, are summarized in Table 2. For all the adsorption sites, the H–H bond lengths d_{H-H} of the H_2 molecule increased slightly from 0.75 Å in the gas phase (Ganji *et al.*, 2014; Yu *et al.*, 2018) to 0.78 Å with increasing Θ values. Furthermore, H_2 was adsorbed on the top, bridge and cavity sites with tilt angles of 17.8°, 47.1° and 55.3°, respectively, at $\Theta = 0.25$ ML. The angles on these adsorption sites decreased with increasing coverage. By contrast, the H–H bonds of H_2 molecules adsorbed

https://doi.org/10.1180/clm.2018.28 Published online by Cambridge University Press

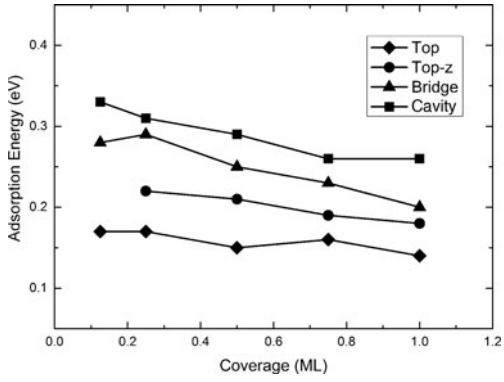

FIG. 3. Calculated adsorption energy (E_{ads}) of the H_2/kaolinite (001) surface *vs*. the coverage for the H_2 molecule adsorption in various sites. The solid lines connecting the calculated adsorption energies are used as visual guides. ML = monolayer.

on the top-z sites were almost perpendicular to the surface with angles of ~90° for coverage $0 < \Theta \leq 1$ ML. With respect to the height h_{H_2-H} of adsorbate H_2 above the kaolinite surface, for the cavity adsorption site, the value of h_{H_2-H} was slightly smaller than that for the top, top-z and bridge sites at the coverage range of $1/4 \leq \Theta \leq 1$ ML (Table 2). A short height h_{H_2-H} implied a strong interaction between H_2 and the kaolinite surface. Also, the cavity sites were the most stable. The calculated adsorbate height of H_2 on these four types of surface sites are illustrated for different coverages in the regime $1/4 \leq \Theta \leq 1$ ML (Fig. 4). Note that for all four types of adsorption sites, the values of h_{H_2-H} increased with increasing Θ, which was consistent with the fact that the stability of adsorbed H_2 decreased with increasing coverage.

During geometry optimization, the distances between the interlayer of the outermost three atomic layers of kaolinite were changed. The changes of Δd_{ij} were calculated according to the equation $\Delta d_{ij} = (d_{ij} - d_0) / d_0$, where d_{ij} and d_0 are the distance between the ith and jth layers of the relaxed surface and the corresponding distance between the ith and jth layer of the clean kaolinite along the (001) direction, respectively. The calculated relaxations for the kaolinite (001) surface are summarized in Table 3. The calculated results showed that the adsorption of H_2 on kaolinite (001) induced notable changes in the interlayer distance of the substrate. After adsorption of H_2 molecules at the top and top-z sites, the distance between the first and second layer, Δd_{12}, was positive from 0.39% to 0.57% and from 0.83% to 1.88%, but the Δd_{23} decreased from 0.16% to 0.13% and from 0.11% to 0.06%, respectively, for coverage $0 < \Theta \leq 1$ ML. Therefore, the distance between the topmost two atomic layers expanded, but the distance between the second and third layers of the kaolinite (001) surface contracted with increasing H_2 coverage. Analogously, for the bridge and cavity sites, the Δd_{12} was negative from –3.44% to –1.92% and –2.38% to –0.80%, and the Δd_{23} increased from –0.31% to –0.13% and –0.06% to 0.01% with increasing H_2 coverage, respectively. These changes reflected the strong influence of the H_2 adsorbates on the neighbouring H and O atoms and, thus, resulted from significant redistribution of the electronic structure. H_2 adsorption caused the outermost kaolinite (001) layer separation to relax back to something close to its 'ideal' bulk value.

To gain more insights into the precise nature of the chemisorbed molecular state in the H_2/kaolinite (001) system, the electronic partial density of state (PDOS) of the H_2 molecule and the neighbouring H and O atoms of the (001) surface were calculated. The results were analysed by means of the electron density difference $\Delta\rho(r)$, which was obtained by subtracting the electron densities of non-interacting component systems, $\rho_{kaolinite(001)}(r) + \rho_{H_2}(r)$, from the density $\rho(r)$ of the H_2/kaolinite (001) system, while retaining the atomic

TABLE 1. The calculated adsorption energy (E_{ads}, eV), as a function of molecular H_2 coverage on the various sites of kaolinite (001).

Site	ML0.0625	ML0.125	ML0.25	ML0.5	ML0.75	ML1.0
Top	–	0.17	0.17	0.15	0.16	0.14
Top-z	–	–	0.22	0.21	0.19	0.18
Bridge	–	0.28	0.29	0.25	0.23	0.20
Cavity	0.39	0.33	0.31	0.29	0.26	0.26

ML = monolayer.

https://doi.org/10.1180/clm.2018.28 Published online by Cambridge University Press

TABLE 2. The calculated adsorbate heights (h_{H_2-H}), angles of the H–H bond with the surface (∠HHS) and H–H bond lengths ($d_{H\text{-}H}$) for various coverages of atomic H_2 adsorption on the kaolinite (001) surface.

	h_{H_2-H} (Å)				∠HHS (°)				d_{H-H} (Å)			
Coverage Θ (ML)	0.25	0.5	0.75	1.0	0.25	0.5	0.75	1.0	0.25	0.5	0.75	1.0
Top	1.69	1.74	1.74	1.77	17.8	17.1	14.5	14.4	0.771	0.778	0.776	0.777
Top-z	1.54	1.56	1.55	1.61	88.9	89.3	89.7	89.8	0.781	0.780	0.783	0.782
Bridge	1.23	1.33	1.49	1.47	47.1	46.6	46.0	45.6	0.780	0.781	0.779	0.783
Cavity	1.26	1.31	1.42	1.40	55.3	54.9	54.1	53.4	0.781	0.784	0.782	0.781

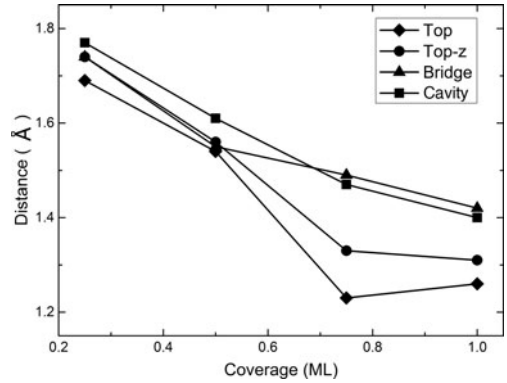

FIG. 4. Calculated adsorbate height, h_{H_2-H}, of H_2 above the surface *vs*. the coverage for the H_2 molecule adsorption on various sites. The solid lines connecting the calculated heights are used as visual guides. ML = monolayer.

positions of the component system at the same location as in H_2/kaolinite (001). Positive (dark) $\Delta\rho(r)$ values indicated an accumulation of electron density upon binding, while negative (grey) values corresponded to electron density depletion.

As a typical example, the PDOSs of the adsorbed H_2 orbitals (*s* and *p*) and the substrate H and O atoms coordinated with H_2 on the two stable adsorption configurations of the top (T_1–T_2) and cavity sites were plotted (Fig. 5); the electron density differences are shown in Figs 5a and c (insets). For comparison, the PDOSs of the free H_2 molecule and the corresponding neighbouring O and H atoms of clean kaolinite (001) surface were also calculated. After adsorption of the H_2 molecule on the top site of kaolinite (001), both the *s* and *p* orbitals of H_2 shifted down in energy by ~4.9 eV. Furthermore, the amplitudes of *sp* bonding orbitals were weaker than those in the free H_2. By contrast, the *sp* orbitals of the surface H and O atoms had a small shift upwards with respect to the Fermi level. As the *sp* orbitals of adsorbed H_2 aligned with the *p* bonding orbital of the adsorbed neighbouring O atom of kaolinite (001), the energy ranged from –6.72 to –4.77 eV (Figs 5a, b). These features were essentially caused by the different electronegativities of kaolinite and H_2 molecules, which induced charge redistribution and thus built a global electrostatic attraction between the H_2 molecule and neighbouring H and O atoms. The result was substantiated by the 3D electron density difference (inset of Fig. 5a). A remarkable charge accumulation existed between the adsorbate and substrate and an H–H bond was formed.

The PDOS of the tilted H_2 adsorbed on a cavity site is depicted in Fig. 5c and d. A new peak at –

https://doi.org/10.1180/clm.2018.28 Published online by Cambridge University Press

TABLE 3. The calculated interlayer relaxations (Δd_{12} and Δd_{23}) for various coverages of atomic H_2 adsorption on the kaolinite (001) surface.

	Δd_{12} (%)				Δd_{23} (%)			
Coverage Θ (ML)	0.25	0.5	0.75	1.0	0.25	0.5	0.75	1.0
Top	0.39	0.39	0.48	0.57	0.16	0.140	0.140	0.13
Top-z	0.83	1.21	1.43	1.88	0.11	0.07	0.03	0.06
Bridge	−3.44	−2.89	−2.40	−1.92	−0.31	−0.30	−0.16	−0.13
Cavity	−2.38	−2.68	−1.13	−0.80	−0.09	−0.06	0.00	0.01

ML = monolayer.

5.76 eV below the Fermi level was observed in the PDOS. This new peak was contributed by the *s* hybridization with kaolinite *s* and *p* orbitals. The orbitals of the H_2 molecule were shifted to lower energy and the amplitudes of the *sp* orbitals were weaker than those in a free H_2 molecule, even in the H_2 adsorbed on the top site. Furthermore, the overlap between adsorbed H_2 and neighbouring O and H atoms of kaolinite (001) surface electrons in the energy ranged from –6.69 to –3.27 eV. The 3D electron density difference distribution of H_2 was calculated (Fig. 5c, inset), which revealed the redistribution of charge after adsorption. For adsorption in cavity sites, the charge depletion was mainly distributed around the H atoms of the kaolinite (001) surface, while a manifested charge accumulation was observed in the H atoms of H_2, displaying acceptance of electrons from the *sp* states of surface H and O atoms. The above results illustrated that the cavity was more stable than the top adsorption site for H_2 molecules.

The orbital-resolved PDOS for the H_2 adsorption on the bridge site and the neighbouring O and H atoms at Θ = 1/8 and Θ = 1 ML are shown in Fig. 6a and b, respectively. At a high coverage (Θ = 1 ML), the narrow amplitude peak at – 5.37 eV denoted the 'H_2 *s* state' (Fig. 6b), which was mainly hybridized with the *sp* state of the neighbouring H and O atoms of the (001) surface. At a low coverage (Θ = 1/8 ML), the amplitudes of the *sp* orbitals of H_2 molecules were much weaker than those in the case of Θ = 1 ML. Furthermore, compared to Θ = 1 ML, the hybridization of H_2 *s* and surface H and O *sp* states was distinctly enhanced in the case of Θ = 1/8 ML. In particular, the main peak at $E = \sim -4.59$ eV in the H_2 *s* PDOS (Fig. 6a) resulted from the hybridization between adsorbate and substrate. The new H_2 peak at – 6.01 eV below the Fermi level observed in Fig. 6a showed that the peak was contributed by the *s* hybridization with kaolinite *s* and *p* orbitals. These results revealed that the *s* orbital hybridized strongly with kaolinite *sp* orbitals and that the covalent H–H bond between H_2 molecules and the kaolinite (001) surface decreased with the increasing coverage of H_2 molecules.

CONCLUSIONS

The first-principles total energy calculation was used to investigate systematically the mechanism of H_2 molecule adsorption on the kaolinite (001) surface, the adsorption energy and the changes in atomic and electronic structures. Different adsorption sites have

https://doi.org/10.1180/clm.2018.28 Published online by Cambridge University Press

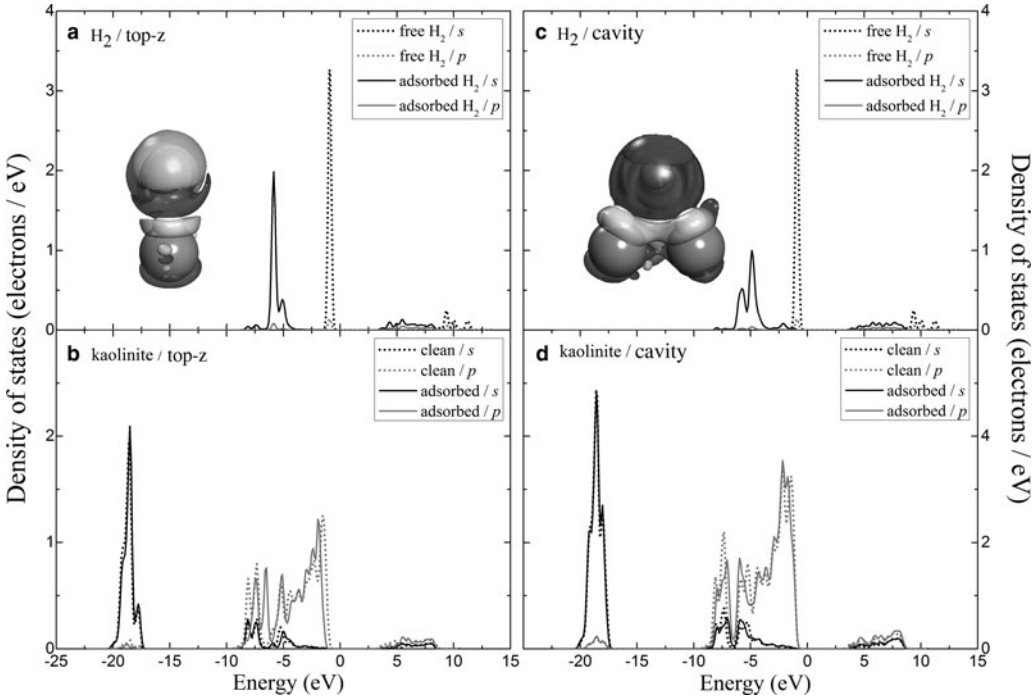

FIG. 5. The partial density of state plots for the H_2 molecule and the neighbouring O and H atoms bonded to H_2 at the stable top and cavity adsorption sites on the surface: (a) free and adsorbed H_2 molecule at the top adsorption site; (b) clean and adsorbed kaolinite (001) surface at the top adsorption site; (c) free and adsorbed H_2 molecule at the cavity adsorption site; (d) clean and adsorbed kaolinite (001) surface at the cavity adsorption site. The insets show the side views of electron density differences for the H_2 atoms at the stable (a) top and (c) cavity adsorption sites. The Fermi energy is set at zero.

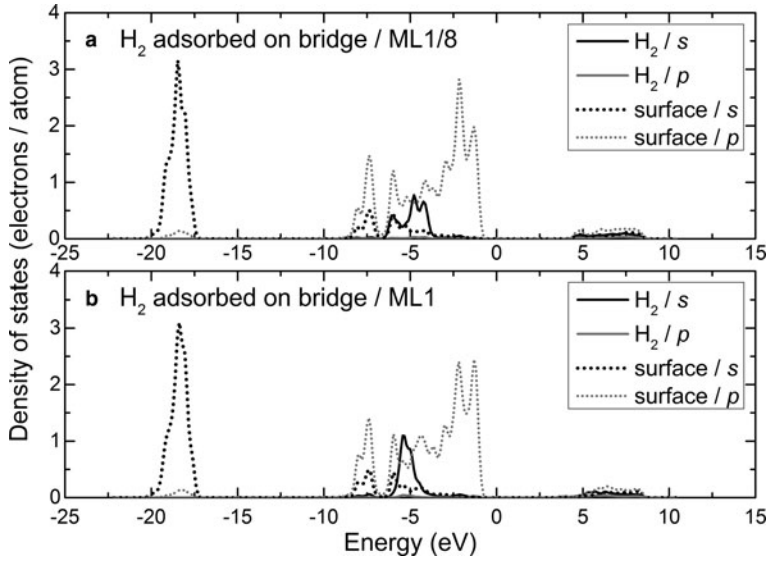

FIG. 6. The partial density of state plots for the bridge adsorption site on a surface H_2 molecule and the neighbouring H and O atoms at (a) $\Theta = 1/8$ and (b) $\Theta = 1$ ML, respectively. The Fermi level is set at zero. ML = monolayer.

https://doi.org/10.1180/clm.2018.28 Published online by Cambridge University Press

been considered using surface models (p [2 × 2] surface unit cells) in a wide range of coverage from 1/16 to 1 ML. The three-fold cavity site is the most stable among all possible pure adsorbtion sites, followed by the bridge, top-z and top sites. Adsorption energy at the most stable position was obviously greater than at the other adsorption sites at the same coverage. Remarkably, this influence on the energy decreased with increasing H_2 coverage. The decrease in the H_2 adsorption energy for all four types of sites in the coverage range $0 < \Theta \leq 1$ implied the lower stability of surface adsorption due to the repulsion of neighbouring H_2 molecules. Different coverage has obvious effects on the atomic geometry, the charge density distribution and the electronic structure of the adsorbed H_2 on the kaolinite (001) surface. The H–H bond lengths $d_{H–H}$ of the H_2 molecule on all adsorption sites increased slightly from 0.75 Å in the gas phase to 0.78 Å with increasing Θ values. The distances between the interlayers of the three outermost atomic layers of kaolinite changed significantly, which underlined the fundamental influence of covalent bonding between the H_2 molecule and kaolinite surface H atoms. Furthermore, the changes in the orbital-resolved PDOS and the distribution of electron density difference of H_2 and O and H atoms of the surface were smaller with increasing coverage, which indicated that the hydrogen molecules are easily adsorbed with lower coverage. The above results will be helpful for future theoretical studies of the adsorption behaviour of H_2 on the kaolinite (001) surface, which is of key importance in H_2 storage.

ACKNOWLEDGMENTS

This research was supported by the National Key Research and Development Program (No. 2016YFC060090X), the Program for the National Natural Science Foundation of China (No. 41702317 and 51574296) and the Young Elite Scientist Sponsorship Program by the Chinese Association for Science and Technology (CAST).

REFERENCES

Adams J.M. (1983) Hydrogen atom position in kaolinite by neutron profile refinement. *Clays and Clay Minerals*, **31**, 352–358.

Alver B.E. (2017) Adsorption studies of hydrogen and ethylene on cation-exchanged bentonite. *Clay Minerals*, **52**, 67–73.

Areán C.O., Palomino G.T., Carayol M.R.L., Pulido A., Rubeš M., Bludský O. & Nachtigall P. (2009) Hydrogen adsorption on the zeolite Ca-A: DFT and FT-IR investigation. *Chemical Physics Letters*, **477**, 139–143.

Bachurin D.V. & Viadimirov P.V. (2017) *Ab initio* study of beryllium surfaces with different hydrogen coverages. *Acta Materialia*, **134**, 81–92.

Bailey S.W. (1980) Structure of layer silicates, Pp. 36–123 in: *Crystal Structures of Clay Minerals and Their X-ray Identification*. (G.W. Brindley & G. Brown, editors). Mineralogical Society, London, UK.

Benco L., Tunega D., Hafner J. & Lischka H. (2001) Orientation of OH groups in kaolinite and dickite: *ab initio* molecular dynamics study. *American Mineralogist*, **86**, 1057–1065.

Bish D.L. (1993) Rietveld refinement of the kaolinite structure at 1.5 K. *Clays and Clay Minerals*, **41**, 738–744.

Blöchl P.E. (1994) Projector augmented-wave method. *Physical Review B*, **50**, 17953–17979.

Brigatti M.F., Galan E. & Theng B.K.G. (2006) General introduction: clays, clay minerals, and clay science. Pp. 27–30 in: *Handbook of Clay Science* (F. Bergaya, B.K.G. Theng & G. Lagaly, editors). Elsevier Ltd, New York, NY, USA.

Charlet L., Alt-Epping P., Wersin P. & Gilbert B. (2017) Diffusive transport and reaction in clay rocks: a storage (nuclear waste, CO_2 H_2), energy (shale gas) and water quality issue. *Advances in Water Resources*, **106**, 39–59.

Chen Y.H. & Lu D.L. (2015) H_2 capture by kaolinite and its adsorption mechanism. *Applied Clay Science*, **104**, 221–228.

Fayaz H., Saidur R., Razali N., Anuar F.S., Saleman A.R. & Islam M.R. (2012) An overview of hydrogen as a vehicle fuel. *Renewable and Sustainable Energy Reviews*, **16**, 5511–5528.

Ganji M.D., Sharifi N., Ahangari M.G. & Khosravi A. (2014) Density functional theory calculations of hydrogen molecule adsorption on monolayer molybdenum and tungsten disulfide. *Physica E*, **57**, 28–34.

Giese R.F., Jr (1973) Interlayer bonding in kaolinite, dickite, and nacrite. *Clays and Clay Minerals*, **21**, 145–149.

Gu C., Gao G.H. & Yu Y.X. (2004) Density functional study of the adsorption of hydrogen in carbon nanotube. *Journal of the Chinese Rare Earth Society*, **22**, 97–100.

Hajjaji W., Andrejkovicova S., Pullar R.C., Tobaldi D.M., Lopez-Galindo A., Jammousi F., Rocha F. & Labrincha J.A. (2016) Effective removal of anionic and cationic dyes by kaolinite and TiO_2/kaolinite composites. *Clay Minerals*, **51**, 19–27.

Hayashi S. (1997) NMR study of dynamics and evolution of guest molecules in kaolinite/dimethyl sulfoxide intercalation compound. *Clays and Clay Minerals*, **45**, 724–732.

https://doi.org/10.1180/clm.2018.28 Published online by Cambridge University Press

He M.C., Zhao J. & Li Y. (2014) First principles *ab initio* study of CO_2 adsorption on the kaolinite(001) surface. *Clays and Clay Minerals*, **62**, 153–160.

Henkel S., Pudlo D., Werner L., Enzmann F., Reitenbach V., Albrecht D., Würdemann H., Heister K., Ganzer L. & Gaupp R. (2014) Mineral reactions in the geological underground induced by H_2 and CO_2 injections. *Energy Procedia*, **63**, 8026–8035.

Hess A.C. & Saunders V.R. (1992) Periodic *ab initio* Hartree–Fock calculation of the low-symmetry mineral kaolinite. *The Journal of Physical Chemistry*, **11**, 4367–4374.

Hobbs J.D., Cygan R.T., Nagy K.L., Schultz P.A. & Sears M.P. (1997) All-atom *ab initio* energy minimization of the kaolinite crystal structure. *American Mineralogist*, **82**, 657–662.

Hörtz P., Ruff P. & Schäfer R. (2015) A temperature dependent investigation of the adsorption of H_2 on Pt (111) using low-temperature single crystal adsorption calorimetry. *Surface Science*, **639**, 66–69.

Hu X.L. & Michaelides A. (2008) Water on the hydroxylated (001) surface of kaolinite: from monomer adsorption to a flat 2D wetting layer. *Surface Science*, **602**, 960–974.

Itadania A., Tanaka M., Abe T., Taguchi H. & Nagao M. (2007) Al-pillared montmorillonite clay minerals: low-pressure H_2 adsorption at room temperature. *Journal of Colloid and Interface Science*, **313**, 747–750.

Kresse G. & Furthmüller J. (1996) Efficient iterative schemes for *ab initio* total-energy calculations using a plane-wave basis set. *Physical Review B*, **54**, 11169–11173.

Kresse G. & Joubert J. (1999) From ultrasoft pseudopotentials to the projector augmented-wave method. *Physical Review B*, **59**, 1758–1762.

Mahdi R.S. & Sahar Y. (2015) Theoretical study of adsorption of H_2 gas on pristine and AsGa-doped (4, 4) armchair models of BPNTs. *Computational Condensed Matter*, **3**, 21–29.

Mondelli C., Bardelli F., Vitillo J.G., Didier M., Brendle J., Cavicchia D.R., Robinet J.C. & Charlet L. (2015) Hydrogen adsorption and diffusion in synthetic Na-montmorillonites at high pressures and temperature. *International Journal of Hydrogen Energy*, **40**, 2698–2709.

Monkhorst H.J. & Pack J.D. (1976) Special points for Brillouin-zone integrations. *Physical Review B*, **13**, 5188–5192.

Niaz S., Manzoor T. & Pandith A.H. (2015) Hydrogen storage: materials, methods and perspectives. *Renewable and Sustainable Energy Reviews*, **50**, 457–469.

Plançon A., Giese R.F., Jr, Snyder R., Drits V.A. & Bookin A.S. (1997) Stacking faults in the kaolinite-group minerals: defect structures of kaolinite. *Clays and Clay Minerals*, **37**, 195–198.

Ren J.W., Musyoka N.M., Langmi H.W., Mathe M. & Liao S.J. (2017) Current research trends and perspectives on materials-based hydrogen storage solutions: a critical review. *International Journal of Hydrogen Energy*, **42**, 289–311.

Roszak R., Firlej L., Roszak S., Pfeifer P. & Kuchta B. (2016) Hydrogen storage by adsorption in porous materials: is it possible? *Colloids and Surfaces A: Physicochemical and Engineering Aspects*, **496**, 69–76.

Saada A., Gaboriau H., Cornu S., Bardot F., Villieras F. & Croue J.P. (2003) Adsorption of humic acid onto a kaolinitic clay studied by high-resolution argon adsorption volumetry. *Clay Minerals*, **38**, 433–443.

Sato H., Ono K., Johnston C.T. & Yamagishi A. (2005) First-principles studies on the elastic constants of a 1:1 layered kaolinite mineral. *American Mineralogist*, **90**, 1824–1826.

Shervani S., Mukherjee P., Gupta A., Mishra G., Illath K., Ajithkumar T.G., Sivakumar S., Sen P., Balani K. & Subramaniam A. (2017) Multi-mode hydrogen storage in nanocontainers. *International Journal of Hydrogen Energy*, **42**, 24256–24262.

Sigot L., Ducom G. & Germain P. (2016) Adsorption of hydrogen sulfide (H_2S) on zeolite (Z): retention mechanism. *Chemical Engineering Journal*, **287**, 47–53.

Šolc R., Gerzabek M.H., Lischka H. & Tunega D. (2011) Wettability of kaolinite (001) surfaces – molecular dynamic study. *Geoderma*, **169**, 47–54.

Sun Q.Q., Yang T.L., Yang L., Fan K., Peng S.M., Long X. G., Zhou X.S., Zu X.T. & Du J.C. (2016) First-principles study on the adsorption and dissociation of H_2 molecules on Be(0001) surfaces. *Computational Condensed Matter*, **117**, 251–258.

Teppen B.J., Rasmussen K., Bertsch P.M., Miller D.M. & Schäferll L. (1997) Molecular dynamic modeling of clay minerals. 1. Gibbsite, kaolinite, pyrophyllite, and beidellite. *Journal of Physical and Chemical B*, **101**, 1579–1587.

Venaruzzo J.L., Volzone C., Rueda M.L. & Ortida J. (2002) Modified bentonitic clay minerals as adsorbents of CO, CO_2, and SO_2 gases. *Microporous Mesoporous Materials*, **56**, 73–80.

Wei T.Y., Lin K.L., Tseng Y.S. & Chan S.L.I. (2017) A review on the characterization of hydrogen in hydrogen storage materials. *Renewable and Sustainable Energy Reviews*, **79**, 1122–1133.

Xie W.W., Peng L., Peng D.L., Gu F.L. & Liu J. (2014) Process of H_2 adsorption on Fe(110) surface: a density functional theory study. *Applied Surface Science*, **296**, 47–52.

Yu M.T., Liu L.L., Wang Q., Jia L.T., Hou B., Si Y.B., Li D.B. & Zhao Y. (2018) High coverage H_2 adsorption and dissociation on fcc Co surfaces from DFT and thermodynamics. *International Journal of Hydrogen Energy*, **43**, 5576–5590.

Zhang W.B., Zhang S.L., Zhang Z.J., Wang L.L. & Yang W. (2014) The hydrogen adsorption on Zr-decorated LiB(001): a DFT study. *Vacuum*, **110**, 62–68.

https://doi.org/10.1180/clm.2018.28 Published online by Cambridge University Press